Optics and Lasers in Engineering 102 (2018) 136–142

Contents lists available at ScienceDirect

Optics and Lasers in Engineering

journal homepage: www.elsevier.com/locate/optlaseng

Circular carrier squeezing interferometry: Suppressing phase shift error in simultaneous phase-shifting point-diffraction interferometer

Donghui Zheng[a,b], Lei Chen[a,*], Jinpeng Li[c], Qinyuan Sun[a], Wenhua Zhu[a], James Anderson[b], Jian Zhao[b], Axel Schülzgen[b]

[a] School of Electronic and Optical Engineering, Nanjing University of Science & Technology, Nanjing 210094, China
[b] CREOL, The College of Optics and Photonics, University of Central Florida, Orlando, FL 32816, USA
[c] Nanjing Astronomical Instruments Co., Ltd., Chinese Academy of Sciences, Nanjing 210042, China

ARTICLE INFO

Keywords:
Circular carrier
Interferometry
Point-diffraction
Phase-shifting

ABSTRACT

Circular carrier squeezing interferometry (CCSI) is proposed and applied to suppress phase shift error in simultaneous phase-shifting point-diffraction interferometer (SPSPDI). By introducing a defocus, four phase-shifting point-diffraction interferograms with circular carrier are acquired, and then converted into linear carrier interferograms by a coordinate transform. Rearranging the transformed interferograms into a spatial-temporal fringe (STF), so the error lobe will be separated from the phase lobe in the Fourier spectrum of the STF, and filtering the phase lobe to calculate the extended phase, when combined with the corresponding inverse coordinate transform, exactly retrieves the initial phase. Both simulations and experiments validate the ability of CCSI to suppress the ripple error generated by the phase shift error. Compared with carrier squeezing interferometry (CSI), CCSI is effective on some occasions in which a linear carrier is difficult to introduce, and with the added benefit of eliminating retrace error.

© 2017 Elsevier Ltd. All rights reserved.

1. Introduction

Point diffraction interferometer (PDI) [1] is widely used in optical manufacturing and testing [2,3], adaptive optics [4,5], phase microscopy [6,7], etc., due to its simple, self-referencing construction. However, this same, desirable characteristic, makes the introduction of phase-shifting technology difficult. One method of achieving this was provided by Kadono, who constructed a pinhole in a linear polarizer and combined with some polarization optics, to realize a phase-shifting PDI [8]. Later, he developed a second phase-shifting PDI by etching a small pinhole in the electrodes of a liquid-crystal variable retarder, and analyzed the potential errors [9]. And Guardalben analyzed the frame-to-frame intensity changes and alignment distortions of the host liquid crystal [10]. Wyant manufactured a polarization point-diffraction plate (PPDP), which is a pinhole etched into a thin-film half-wave plate by using focused ion beam, and realized phase-shifting with an electro-optic modulator, also, the errors in the alignments and retardances of polarization optics are explained [11]. In these cases, the measurements contain a temporal phase-shifting process, and will be influenced by vibration and so on [12], so some work had been done to achieve real-time measurement. Based on the diffraction properties of a grating and a pinhole, Kwon fabricated a pinhole in a sinusoidal transmission grating to produce three simultaneous phase-shifting interferograms, but it exists intensity consistency error between the interferograms to some extent [13]. Later, by starting with a uniform grid, Millerd, and Wyant et al. created another PPDP by using focused ion beam milling and selectively removing material. By coupling the PPDP with an optical configuration that produces four phase-shifting interferograms on a single CCD sensor, a instantaneous phase-shift point-diffraction interferometer was accomplished [14]. Most recently, Lei Chen et al. set up a similar system, by making a pinhole on the metallic wires layer of a wire grid polarizer, which was combined with a simultaneous phase-shifting system, to realize a spatial phase-shifting polarization interferometer, they also analyzed the diffraction wavefront quality and the retardance error in the system [15].

Most of the systems mentioned above adopted some polarization optics and beam splitters, such as retarders, or gratings. That means the optical axis alignment error, retardance error, etc. may contribute to the phase-shift error [11,16]. Utilizing the iterative method and statistical technique, some algorithms have been proposed to suppress phase-shift error. Qian proposed an iterative method based on least-squares fittings to retrieve wavefront phase from tilt phase-shift interferograms [17], while Yichun worked to overcome the random piston and tilt wavefront errors generated by the phase shifter [18]. Jianxin used Radon trans-

* Corresponding author.
E-mail address: chenlei@njust.edu.cn (L. Chen).

https://doi.org/10.1016/j.optlaseng.2017.11.002
Received 15 August 2017; Received in revised form 21 October 2017; Accepted 2 November 2017
0143-8166/© 2017 Elsevier Ltd. All rights reserved.

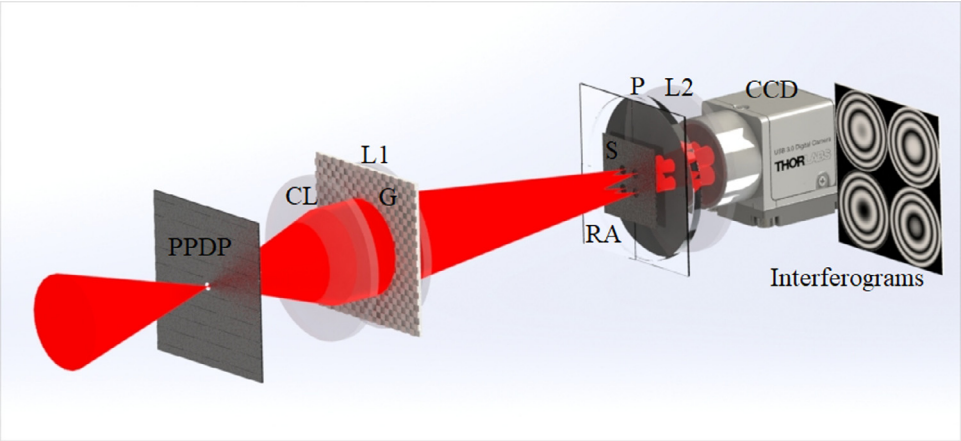

Fig. 1. Diagram of the SPSPDI.

form to extract the phase plane with random tilts, and then retrieved the phase distribution by the least squares method [19]. In contrast, G Lai proposed a generalized phase-shifting interferometry [20], and later, some other scholars improved this method and made some applications. It is a good phase retrieval method for interferograms with random phase-shifts. It can be easily coded without iteration [21–23]. Based on squeezing interferometry [24], Bo Li proposed carrier squeezing interferometry (CSI) to suppress errors from inaccurate phase shift [25], which was later improved by Zhu such that only two interferograms were needed [26]. CSI requires introducing a linear carrier in the interferograms, usually by tilting the reference mirror, which can be difficult when measuring a specimen with large spherical departure or an on-axis asphere with small aspherical departure with a phase-shfting point-diffraction interferometer, because as the focus of the convergent beam deviates from the center of pinhole in the direction perpendicular to the axis, the diffraction beam (reference beam) can't cover the transmission beam (test beam) completely, and it may even generates interferogram between the transmission beam and the first order diffraction ring, these factors will all lead to faulty measurements. But in these situations, circular carrier interferograms are easier to be achieved than linear ones by introducing a defocus in an interferometric setup [2].

In this paper, we propose a circular carrier squeezing interferometry (CCSI) method, and apply it to suppress the phase shift error in a simultaneous phase-shifting point-diffraction interferometer (SPSPDI), the CCSI eliminates the ripple error generated by phase-shift error in phase distribution effectively. It is suitable for some occasions in which CSI is not effective, since tilt is difficult to introduce, for example, phase-shifting point-diffraction interferometers, and also when a specimen with large spherical departure or an on-axis asphere with small aspherical departure is measured. Additionally, there is no retrace error compared to CSI in which a linear carrier is required, usually by tilting the reference mirror, and lead to deviation between reflected light and incident light.

2. Theory

2.1. SPSPDI

As shown by Fig. 1, a convergent beam propagates through a polarization point-diffraction plate (PPDP), which is based on a wire grid polarizer, by manufacturing a pinhole on its metallic wires layer. After a collimating lens (CL), the transmission beam and diffraction beam propagate in parallel to a grating (G), then are focused via a lens (L1), Four diffraction orders with the same diffraction efficiency are selected by a stop (S) at the focal plane of L1, and then pass through a retarder array(RA), which contains four retarders with different retardations of 0, $\pi/2$, π, and $3\pi/2$, respectively, the following is a polarizer (P) and another lens (L2), so we can acquire four simultaneous phase-shifting point-diffraction interferograms.

2.2. Circular carrier squeezing interferometry

In general, the intensity of the n-th interferogram acquired by a phase-shifting interferometer can be expressed by

$$I_n = a(x,y) + b(x,y)\cos\left[\varphi(x,y) + 2\pi f_0 n + \varepsilon_n(x,y)\right], n = 0, 1, \ldots, N-1 \tag{1}$$

where $a(x, y)$ represents the background component, $b(x, y)$ is the contrast, $\varphi(x, y)$ is the initial phase, f_0 is the phase shift frequency which equals $1/N$, and $\varepsilon_n(x, y)$ is the phase shift error of the nth interferogram. By Introducing a defocus into the interferogram, a circular carrier interferogram is acquired, and Eq. (1) can be rewritten as

$$I_n = a(x,y) + b(x,y)\cos\left[2\pi f_c\left(x^2+y^2\right) + \varphi(x,y) + 2\pi f_0 n + \varepsilon_n(x,y)\right], \quad n = 0, 1, \ldots, N-1 \tag{2}$$

where f_c is the circular carrier coefficient, and the coordinate of the circular carrier interferogram center is (0, 0) in the Cartesian coordinate system. Choosing the center to be the original point, a coordinate transform is made using the following equations,

$$\begin{cases} x = \sqrt{\rho}\cos\theta \\ y = \sqrt{\rho}\sin\theta \end{cases} \tag{3}$$

The intensity expression of a circular carrier interferogram can be rewritten in the new coordinate system (ρ, θ), as

$$I_{Qn} = a_Q(\rho,\theta) + b_Q(\rho,\theta)\cos\left[2\pi f_c\rho + \varphi_Q(\rho,\theta) + 2\pi f_0 n + \varepsilon_{Qn}(\rho,\theta)\right], \quad n = 0, 1, \ldots, N-1 \tag{4}$$

where $a_Q(\rho, \theta)$, $b_Q(\rho, \theta)$ and $\varphi_Q(\rho, \theta)$ represents the background, contrast and initial phase in the new (ρ, θ) coordinate system, respectively. In this way, a circular carrier interferogram is converted to a linear carrier interferogram. Rearranging the linear carrier interferograms using,

$$I'(N\rho + n, \theta) = I_{Qn}(\rho, \theta) \tag{5}$$

allows the rearranged Spatial-Temporal Fringe(STF) to be expressed by,

$$I'(\rho',\theta) = a_Q(\rho',\theta) + b_Q(\rho',\theta)\cos\left[2\pi f_c\rho' + \varphi_Q(\rho',\theta) + \varepsilon_Q(\rho',\theta)\right] \tag{6}$$

where

$$\varepsilon_Q(\rho',\theta) = \sum_{n=0}^{N-1}\sum_{m=-\infty}^{\infty}\varepsilon_{Qn}\delta(\rho' - Nm - n, \theta) \tag{7}$$

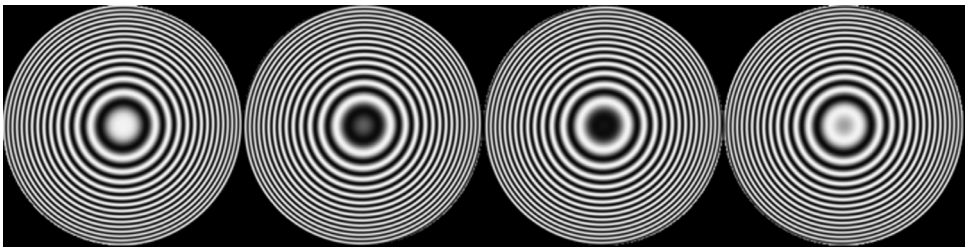

Fig. 2. Simulated interferograms with circular carrier.

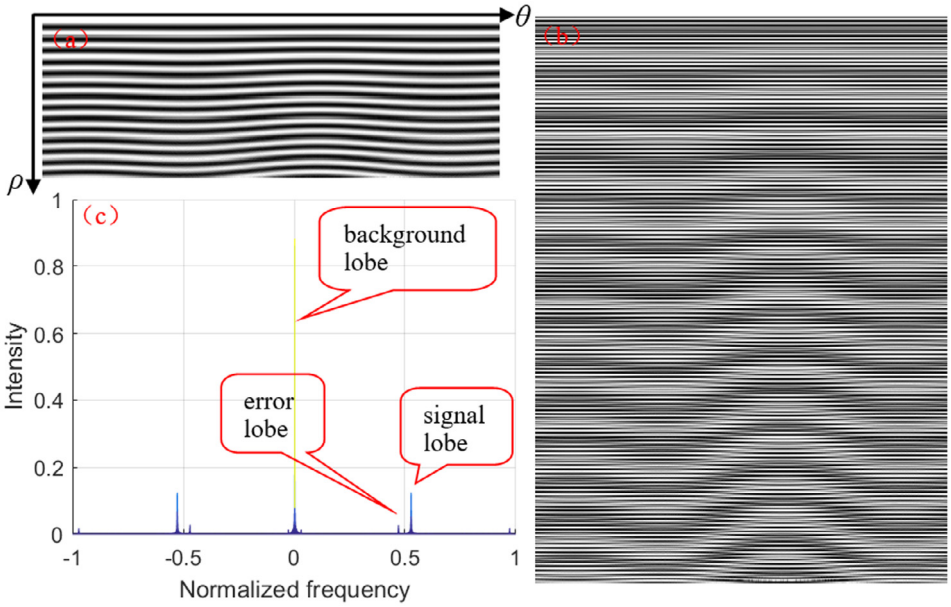

Fig. 3. Transformed interferograms and corresponding spectrum. (a) One of the linear carrier interferograms; (b) STF by squeezing interferometry; (c) Spectrum corresponding to the STF.

Table 1
PV and RMS values of the results in Fig. 4.

	SID4	PSI	CCSI	Difference between PSI and CCSI	PSI residual error	CCSI residual error
PV/λ	0.7086	0.8464	0.7197	0.1241	0.1528	0.0148
RMS/λ	0.1279	0.1437	0.1310	0.0306	0.0323	0.0027

Table 2
PV and RMS values of the results in Fig. 7.

	SID4	PSI	CCSI	Difference between PSI and CCSI	PSI residual error	CCSI residual error
PV/λ	0.3350	0.4269	0.3451	0.2804	0.2572	0.0945
RMS/λ	0.0665	0.0771	0.0705	0.0379	0.0352	0.0161

and $\rho' \in (-NM'/2, NM'/2-1)$, $\theta \in (-N'/2, N'/2-1)$, and (M', N') is the size of the linear carrier interferogram. After making a first order approximation of the trigonometric function in Eq. (6), and then performing a Fourier transform, near the location of f_0, the phase lobe is given by,

$$S(f_0+f_c,0)=\frac{b_Q(\rho',\theta)}{2}\left(1-\sum_{n=0}^{N-1}\frac{\varepsilon_{Qn}}{iN}\right)\Phi_{+1}(f_\rho-f_0-f_c,f_\theta) \tag{8}$$

and the error lobe is given by,

$$S(f_0-f_c,0)=\frac{b_Q(\rho',\theta)}{2}\left(\sum_{n=0}^{N-1}\frac{\varepsilon_{Qn}\exp(-i4\pi n f_0)}{iN}\right)\Phi_{-1}(f_\rho-f_0+f_c,f_\theta) \tag{9}$$

where $\Phi_{\pm1}(f_\rho, f_\theta) = FT[\exp(\pm i\varphi_Q(\rho', \theta))]$, and $FT[\cdot]$ is the Fourier transform operator. From Eqs. (8) and (9), we can find that, with the circular carrier f_c, the phase lobe and the error lobe are separated by a distance of $2f_c$, so it is easy to extract the phase lobe with a filter. The extended phase $\varphi_Q(\rho', \theta)$ will be reconstructed using,

$$\varphi_Q(\rho',\theta)+2\pi(f_0+f_c)\rho'=\arctan\left\{\frac{\mathrm{Im}\{FT^{-1}[S(f_0-f_c,0)]\}}{\mathrm{Re}\{FT^{-1}[S(f_0-f_c,0)]\}}\right\} \tag{10}$$

where $FT^{-1}[\cdot]$ represents an inverse Fourier transform, and the initial phase $\varphi_Q(\rho, \theta)$ can be acquired by,

$$\varphi_Q(\rho,\theta)=\varphi_Q\left(\mathrm{int}\left[\frac{\rho'}{N}\right],\theta\right) \tag{11}$$

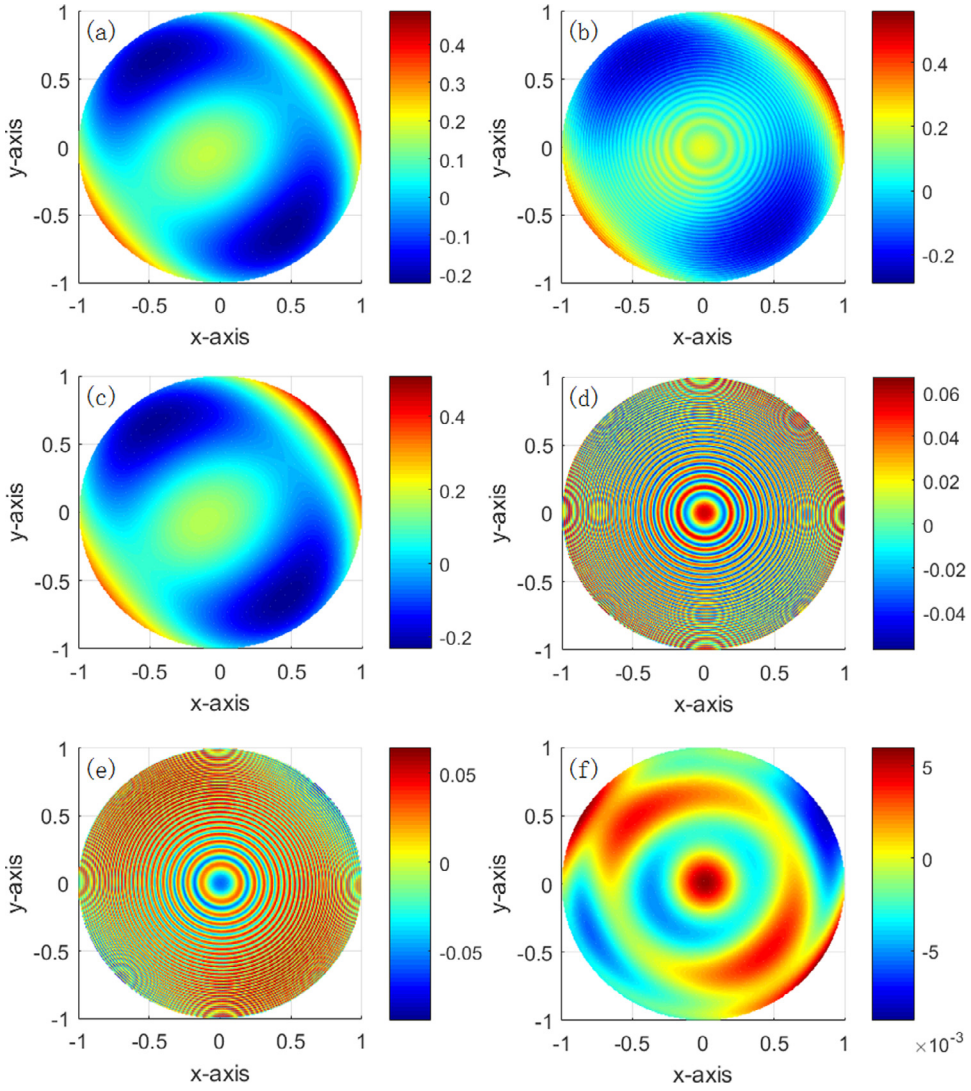

Fig. 4. Simulation results. (a) Standard phase distribution; (b) result of four-bucket algorithm; (c) result of CCSI; (d) difference between (b) and (c); (e) residual error between (a) and (b); (f) residual error between (a) and (c). All phase values are normalized by the wavelength.

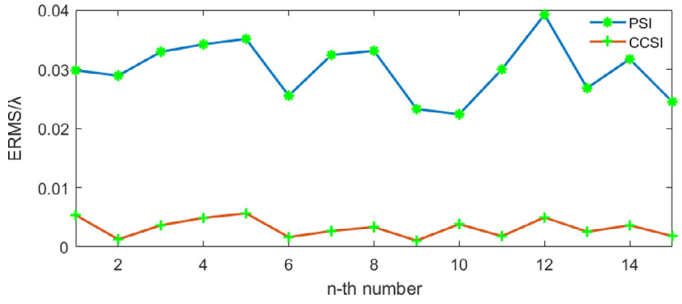

Fig. 5. Root-mean-square value of the residual error, RMSE, providing a direct comparison of the precision of the proposed CCSI method with the conventional PSI method.

where int[·] represents the round operator. After performing an inverse coordinate transform according to Eq. (3), we can get the initial phase $\varphi(x, y)$.

3. Simulation

With this theoretical background, we conducted the relevant numerical simulations. As shown by Fig. 2, four phase-shifting point-diffraction interferograms are generated, the phase shifts of the interferograms are 0, $\pi/2$, π, and $3\pi/2$, and include different phase shift errors. The phase distribution is simulated by Zernike polynomials. It contains defocus, coma, astigmatism, and spherical aberrations, allows the polynomials to be expressed by,

$$z_{foc} = k_1\left[2\left(x^2 + y^2\right)\right] \tag{12}$$

$$z_{com} = k_2\left[-2x + 3x\left(x^2 + y^2\right) - 2y + 3y\left(x^2 + y^2\right)\right] \tag{13}$$

$$z_{ast} = k_3\left[\left(y^2 - x^2\right) + 2xy\right] \tag{14}$$

$$z_{sph} = k_4\left[1 - 6\left(x^2 + y^2\right) + 6\left(x^2 + y^2\right)^2\right] \tag{15}$$

First, a coordinate transform to the interferograms was made, allowing for the conversion of interferograms shown in Fig. 2 into linear carrier interferograms, an example of which is seen in Fig. 3(a). The four linear carrier interferograms are rearranged into a STF, shown in Fig. 3(b), while Fig. 3(c) shows the Fourier spectrum corresponding to the STF. It can be seen from Fig. 3(c) that the phase lobe and the error lobe are separated. Then, the phase lobe was extracted, and combined with the relevant inverse Fourier transform and coordinate transform,

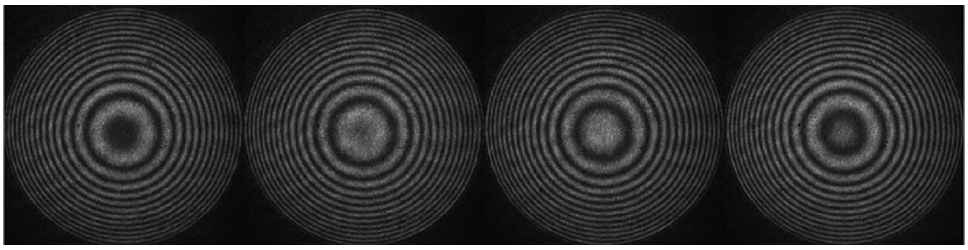

Fig. 6. Circular carrier interferograms.

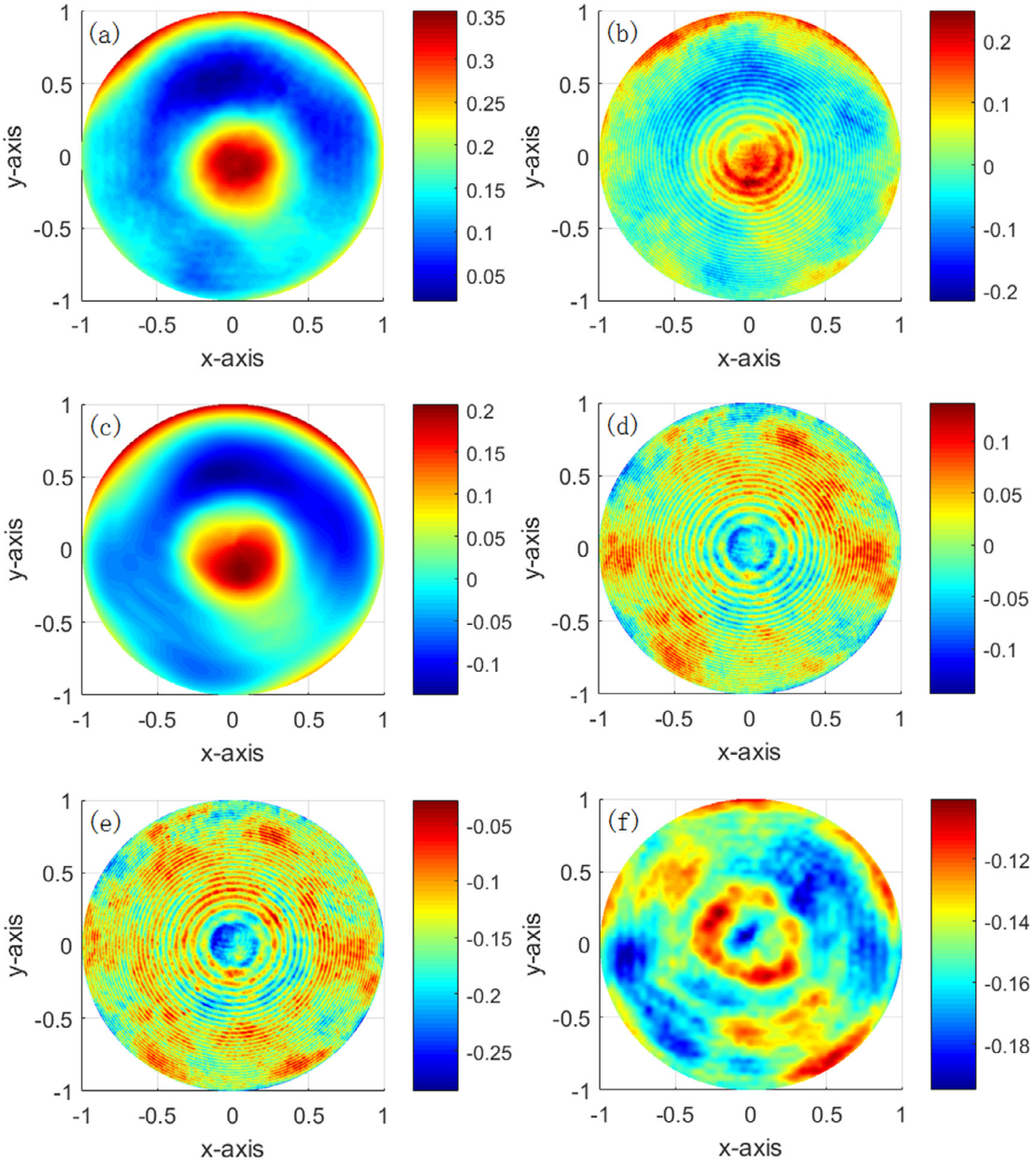

Fig. 7. Experimental results. (a) Measurement result by SID-4; (b) the retrieved phase by PSI; (c) the retrieved phase by CCSI; (d) difference between (b) and (c); (e) PSI residual error: residual error between (b) and (a); (f) CCSI residual error: residual error between (c) and (a). All phase values are normalized by the wavelength.

allowing the initial phase under test to be demodulated, Fig. 4 shows the various simulation results, as well as a comparison of the different simulation methods used.

In Fig. 4, the traditional phase-shifting interferometry (PSI) is adopted for comparison purposes. Fig. 4(a) shows the standard phase distribution. Fig. 4(b) and (c) give results using PSI and CCSI, respectively. Fig. 4(d) shows the difference between the PSI and CCSI, Fig. 4(e) gives the residual error distribution between the PSI and the standard phase, and Fig. 4.(f) is the residual error distribution between the CCSI and the standard phase.Their peak-to valley (PV) and root-mean-square

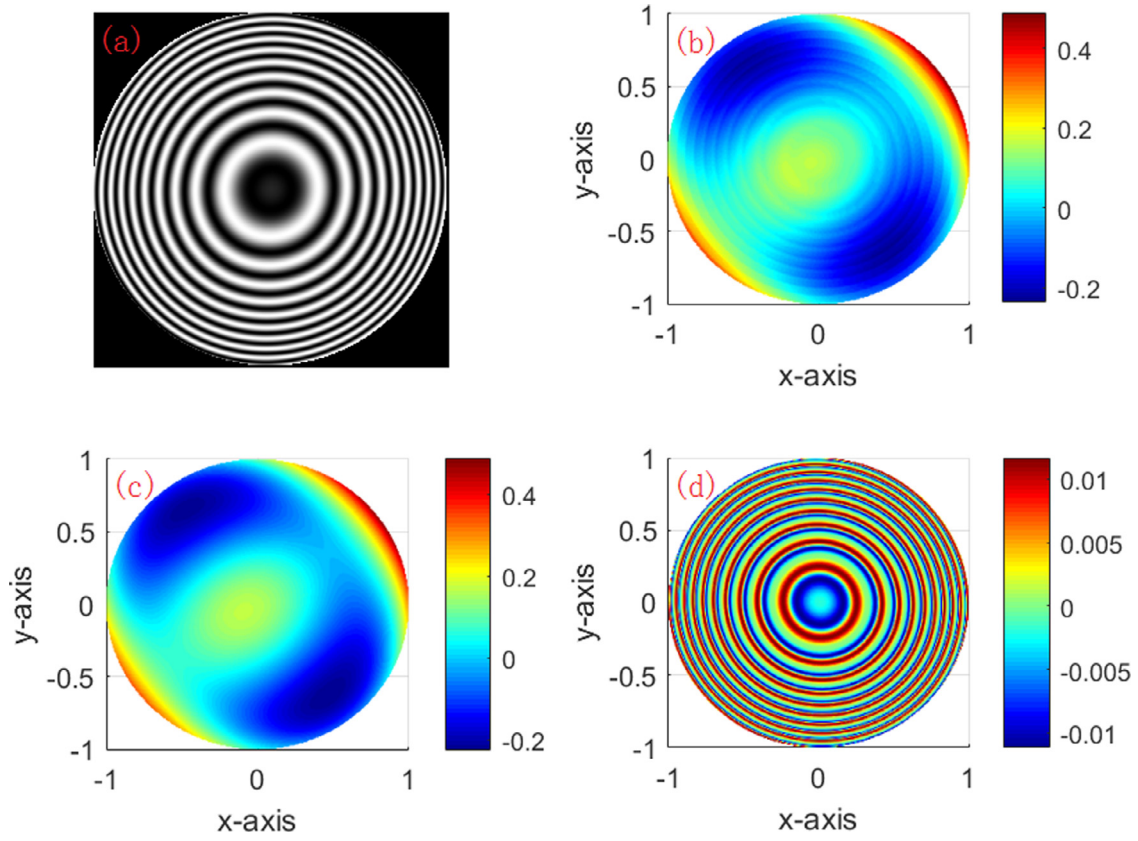

Fig. 8. Intensity distortion analysis. (a) One of the inteferograms; (b) the retrieved phase by PSI; (c) the retrieved phase by CCSI; (d) difference between (b) and (c).

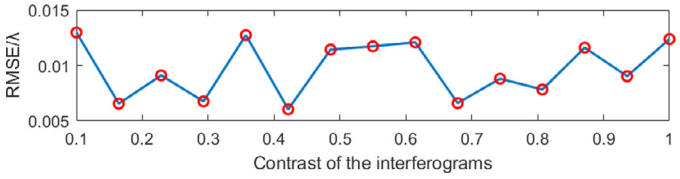

Fig. 9. Retrieved phase error related to the contrast of the interferograms.

(RMS) values are shown in Table. 1. From Fig. 4(b) to (f), it is obvious that, in the phase distribution result using the PSI method, there is a ripple error whose spatial frequency is twice as the fringe frequency of the circular carrier interferograms. Comparitively, the ripple error which is generated by the phase shift error is suppressed well by the proposed CCSI method.

To verify the stability of the proposed CCSI, we repeat the simulations with different phase shift errors (in each simulation, we introduce four different phase shift errors in the four interferograms, respectively.), and use the RMS value of the residual error between the result of CCSI and the standard phase (RMSE) to evaluate the precision of CCSI. The results are shown in Fig. 5, compared with PSI, the precision of CCSI is much better, and the effect of error suppression is obvious.

4. Experiments

An experimental device was set up to measure the transmission wavefront of a collimating lens, with a focal length of 550 mm, and an aperture of 55 mm. The PPDP, which acts as the key component, was manufactured based on a wire grid polarizer using laser ablation, made a pinhole on the metallic wire layer. The retarder array is glued together with four retarders whose retardations are 0, $\pi/2$, π, and $3\pi/2$, respectively, with their fast-axes are all along the horizontal direction. By introducing a defocus along the optical axis, four circular carrier interferograms were captured, as shown in Fig. 6.

By making the relation analysis to the circular carrier interferograms, we get the corresponding results in Fig. 7. Fig. 7(a) is an experimental result which was measured using the SID-4 wavefront sensor manufactured by Phasics corporation in France, which can be viewed as a reference. Fig. 7(b) and (c) are the retrieved phase using PSI and CCSI method, respectively, and Fig. 7(d) shows the difference between the results of PSI and CCSI. To make a further comparison, we analyzed the residuals of the two methods compared to the reference shown in Fig. 7(a), with Fig. 7(e) giving the residual phase distribution of the PSI method, while Fig. 7(f) shows that for the proposed CCSI method. From Fig. 7(b)–(f), we can see that the ripple phase error that appears in the results of the PSI method is strongly suppressed by the CCSI method. Table. 2 shows the PV and RMS values of the results in Fig. 7.

5. Discussion

5.1. Intensity distortion

Considering the light intensity consistency error of the four diffraction orders generated by the grating, we simulated four simultaneous phase shifting interferograms with different intensity, to verify the suppression ability of CCSI for the intensity distortion error. The simulation results are shown in Fig. 8. Fig. 8(a) shows one of the interferograms, and Fig. 8(b) and (c) are the phases retrieved by the PSI method, and the CCSI method, respectively, their difference is shown in Fig. 8(d). It can be seen that the phase error has a same spatial frequency as the fringes, and suppressed by the CCSI method well.

5.2. The circular carrier requirement

To ensure the phase lobe is extracted without being affected by the error lobe, the carrier should provide separation of the lobes in the spectrum of STF. Assume that, the half linewidth of the phase lobe and the error lobe are H and H', respectively. Combining Eqs. (8) and (9), we can get,

$$H' = \frac{R_2}{1+R_1} H \tag{16}$$

where $R_2 = \sum_{n=0}^{N-1} \frac{\varepsilon_{Qn} \exp(-i4\pi n f_0)}{iN}$, $R_1 = -\sum_{n=0}^{N-1} \frac{\varepsilon_{Qn}}{iN}$. Notice that the distance between the two lobes expressed by Eqs. (8) and (9) is $2f_c$, so to separate the two lobes expressed by Eqs. (8) and (9), the circular carrier should satisfy,

$$f_c \geq \frac{H'+H}{2} = \left(1 + \frac{R_2}{1+R_1}\right)\frac{H}{2} \tag{17}$$

At the sametime, we should take the contrast of the interferograms into consideration, since the intensity of the diffraction beam decreases with the defocus, i.e. the circular carrier f_c. We performed some simulations, and the RMSE value is used to evaluate the precision under different contrasts, with the results shown as Fig. 9. It can be seen that the contrast decrease will not result in considerable errors.

6. Conclusion

In this paper, we present a circular carrier squeezing interferometry (CCSI). By introducing a defocus, a group of circular carrier interferograms is obtained, and combined with the coordinate transform and STF techniques, the phase under test can be retrieved and the phase shift error is suppressed effectively. The proposed CCSI method has two following advantages. Firstly, it is particularly suitable for phase-shifting point-diffraction interferometers, also the occasions when measuring a specimen with large spherical departure or an on-axis asphere with small aspherical departure. Secondly, there is no retrace error compared to CSI, which requires a linear carrier, usually by tilting the reference mirror, and lead to deviation between reflected light and incident light.

Acknowledgments

We would like to thank the National Natural Science Foundation of China (No. 61409052, 61505082). Natural Science Foundation of Jiangsu Province (No. BK20160154). National Key Scientific Instrument and Equipment Development Project (2013YQ150829).

References

[1] Smartt RN, Strong J. Point-diffraction interferometer. J Opt Soc Am. 1972;62:726–35.
[2] Malacara D. Optical shop testing. 3rd ed. Wiley; 2007.
[3] Park R, Kim DW, Barret HH. Synthetic phase-shifting for optical testing: point-diffraction interferometry without null optics or phase shifters. Opt Express 2013;21(22):26398–417.
[4] Notaras J, Paterson C. Point-diffraction interferometer for atmospheric adaptive optics in strong scintillation. Opt Commun 2008;281:360–7.
[5] Paterson C, Notaras J. Demonstration of closed-loop adaptive optics with a point-diffraction interferometer in strong scintillation with optical vortices. Opt Express 2007;15:13745–56.
[6] Gao P, Yao B, Min J, Guo R, Zheng J, Ye T, et al. Parallel two-step phase-shifting point-diffraction interferometry for microscopy based on a pair of cube beamsplitters. Opt Express 2011;19(3):1930–5.
[7] Gao P, Harder I, Nercissian V, Mantel K, Yao B. Phase-shifting point-diffraction interferometry with common-path and in-line configuration for microscopy. Opt Lett 2010;35(5):712–14.
[8] Kadono H, Nobukatsu T, Asakura T. New common-path phase shifting interferometer using a polarization technique. Appl Opt 1987;26:898–904.
[9] Kadono H, Ogusu M, Toyooka S. Phase shifting common path interferometer using a liquid-crystal phase modulator. Opt Commun 1994;110:391–400.
[10] Guardalben MJ, Ning L, Jian N, Battaglia DJ, Marshall KL. Experimental comparison of a liguid-crystal point-diffraction interferometer(LCPDI) and a commercial phase-shifting interferometer and methods to improve LCPDI accuracy. Appl Opt 2002;41(7):1353–65.
[11] Neal RM, Wyant JC. Polarization phase-shifting point-diffraction interferometer. Appl Opt 2006;45(15):3463–76.
[12] de Groot PJ. Vibration in phase-shifting interferometry. J Opt Soc Am 1995;12(2):354–65.
[13] Kwon OY. Multichannel phase-shifted interferometer. Opt Lett 1984;9(2):59–61.
[14] Millerd JE, Martinek SJ, Brock NJ, Hayes JB, Wyant JC. Instantaneous phase-shift point-diffraction interferometer. Proc SPIE 2004;5380:422–9.
[15] Zheng D, Li J, Chen L, Zhu W, Han Z, Wulan T, et al. Spatial phase-shifting polarization phase-shifting point-piffraction interferometer for wavefront measurement. Acta Phys Sin 2016;65(11):114203 in Chinese.
[16] Guardalben MJ, Jian N. Phase-shift error as a result of molecular alignment distortions in a liquid-crystal point-diffraction interferometer. Opt Lett 2011;25(16):1171–3.
[17] Liu Q, Wang Y, Ji F, He J. A three-step least-squares iterative method for tilt phase-shift interferometry. Opt Express 2013;21(24):29505–15.
[18] Chen Y, Lin P, Lee C, Liang C. Iterative phase-shifting algorithm immune to random phase shifts and tilts. Appl Opt 2013;52(14):3381–6.
[19] Li J, Zhu R, Chen L, He Y. Phase-tilting interferometry for optical testing. Opt Lett 2013;38(15):2838–41.
[20] Lai G, Yatagai T. Generalized phase-shifting interferometry. J Opt Soc Am A 1991;8(5):822–7.
[21] Patil A, Rastogi P. Approaches in generalized phase shifting interferometry. Opt Las Eng 2005;43:475–90.
[22] Meneses-Fabian C. Self-calibrating generalized phase-shifting interferometry of three phase-steps based on geometric concept of volume enclosed by a surface. J Opt 2016;18:125703.
[23] Yatabe K, Ishikawa K, Oikawa Y. Simple, flexible, and accurate phase retrieval method for generalized phase-shifting interferometry. J Opt Soc Am A 2017;34(1):87–96.
[24] Servin M, Cywiak M, Malacara-Hernandez D, Estrada JC, Quiroga JA. "Spatial carrier interferometry from M temporal phase shifted interferograms: squeezing interferometry. Opt Express 2008;16(13):9276–83.
[25] Li B, Chen L, Wulan T, Ma S, Zhu R. Carrier squeezing interferometry: suppressing phase errors from the inaccurate phase shift. Opt Lett 2011;36(6):996–8.
[26] Zhu RG, Li B, Zhu RH, He Y, Li J. Phase extraction from two phase-shifting fringe patterns using spatial-temporal fringes method. Opt Express 2016;24(7):6814–24.